Review of Scientific Instruments

Development of a hard X-ray split-and-delay line and performance simulations for two-color pump-probe experiments at the European XFEL ⓔⓟ

W. Lu, B. Friedrich, T. Noll, K. Zhou, J. Hallmann, G. Ansaldi, T. Roth, S. Serkez ⓘⓓ, G. Geloni, A. Madsen, and S. Eisebitt

COLLECTIONS

ⓔⓟ This paper was selected as an Editor's Pick

View Online   Export Citation   CrossMark

ARTICLES YOU MAY BE INTERESTED IN

Lock-in Amplifiers up to 600 MHz   Watch

Development of a hard X-ray split-and-delay line and performance simulations for two-color pump-probe experiments at the European XFEL

W. Lu,[1] B. Friedrich,[2] T. Noll,[2] K. Zhou,[3,4,a)] J. Hallmann,[1] G. Ansaldi,[1] T. Roth,[5] S. Serkez,[1] G. Geloni,[1] A. Madsen,[1] and S. Eisebitt[2,6]

[1]*European X-Ray Free-Electron Laser Facility, Holzkoppel 4, 22869 Schenefeld, Germany*
[2]*Max Born Institute, Max-Born-Strasse 2A, 12489 Berlin, Germany*
[3]*Shanghai Institute of Applied Physics, Chinese Academy of Sciences, 201800 Shanghai, China*
[4]*University of Chinese Academy of Sciences, 100049 Beijing, China*
[5]*ESRF—The European Synchrotron, 71 Avenue des Martyrs, 38000 Grenoble, France*
[6]*Institut für Optik und Atomare Physik, Technische Universität Berlin, 10623 Berlin, Germany*

A hard X-ray Split-and-Delay Line (SDL) under construction for the Materials Imaging and Dynamics station at the European X-Ray Free-Electron Laser (XFEL) is presented. This device aims at providing pairs of X-ray pulses with a variable time delay ranging from −10 ps to 800 ps in a photon energy range from 5 to 10 keV for photon correlation and X-ray pump-probe experiments. A custom designed mechanical motion system including active feedback control ensures that the high demands for stability and accuracy can be met and the design goals achieved. Using special radiation configurations of the European XFEL's SASE-2 undulator (SASE: Self-Amplified Spontaneous Emission), two-color hard x-ray pump-probe schemes with varying photon energy separations have been proposed. Simulations indicate that more than 10^9 photons on the sample per pulse-pair and up to about 10% photon energy separation can be achieved in the hard X-ray region using the SDL. *Published by AIP Publishing.*
https://doi.org/10.1063/1.5027071

INTRODUCTION

The intense, ultra-short, and spatially coherent X-ray pulses provided by X-ray Free-Electron Lasers (XFELs) open up areas of research that were previously inaccessible. An X-ray Split-and-Delay Line (SDL) unit gives the opportunity of modifying the pulse pattern leading to new possibilities for photon diagnostics and experiments, for instance, temporal characterization of the XFEL pulses via an auto-correlation measurement and realization of ultrafast x-ray-pump x-ray probe schemes. Additionally, the SDL enables investigations of condensed matter dynamics via correlation spectroscopy and wave-mixing schemes on time scales below the repetition rate of the XFEL. For instance, studies of ultrafast dynamics using various experimental techniques can be performed, e.g., time-resolved X-ray Photon Correlation Spectroscopy (XPCS),[1] Speckle Visibility Spectroscopy (SVS),[2–4] ultrafast X-ray tomography,[5] and temporally and spatially resolved X-ray holography.[6] In addition, with powerful tuneable and synchronized optical laser systems not only X-ray pump X-ray probe experiments but also X-ray probe-optical pump-X-ray probe (XOX)[7] and optical pump-X-ray probe-X-ray probe (OXX) experiments are made possible. Most Free-Electron Laser (FEL) facilities have ongoing projects to develop X-ray SDL systems.[3,8–14]

The Materials Imaging and Dynamics (MID) instrument at the European XFEL facility[15,16] aims at the investigation of nanoscale structures and dynamics by X-ray scattering and imaging. Emphasis is on techniques that exploit the coherence properties of the radiation in combination with the other beam features such as high peak intensity and short pulse duration. Applications to a wide range of materials from hard to soft condensed matter and biological samples are envisaged. The European XFEL facility will provide X-ray pulses separated by 220 ns (4.5 MHz) in 0.6 ms long bunch trains arriving with a repetition rate of 10 Hz.[15] In this fashion, a maximum of 27 000 pulses/s can be delivered for experiments. Special operation modes[17] may permit, in the future, the pulse spacing within the trains to be reduced to ~770 ps (defined by the accelerator RF of 1.3 GHz) for a few pulses per train. Shorter time separation between individual pulses cannot be provided by the accelerator. Hence, in order to access dynamics below 770 ps in the time domain, a SDL unit is required for the MID station.[18,19]

In this article, we report on the concept and mechanical design of the SDL under development. The device is optimized to operate in a photon energy range from 5 to 10 keV and provides pairs of jitter-free X-ray pulses with a variable time delay ranging from −10 ps to 800 ps. Operation at higher photon energy is feasible in a reduced time delay range. This device allows for a window-less integration into the MID beamline. Thus, all optical elements and mechanics, including a laser interferometer setup and about 100 stepper motors, are situated in a particle-free 5×10^{-8} mbar ultra-high vacuum environment. The mechanical concept features separate stages for each optical element to achieve positioning precision in the sub-μm range and tens of nano-radians in angle, while at the same time allowing travels of up to 1 m and angular adjustment ranges of several tens of degrees. Multiple laser interferometers monitor

---

the position of the optical elements and allow an active control of their alignment when changing the delay.

Beyond monochromatic two beam operation, two-colour X-ray pump-probe experiments have recently attracted considerable scientific interest.[20–32] In combination with the broadband radiation configurations available at XFELs,[33–37] a SDL can be used to select two photon energies within the radiation bandwidth and introducing a variable arrival time between these two pulses on the sample, thus enabling time-resolved two-colour hard X-ray pump-probe experiments. Beyond a description of the general SDL design, in this manuscript, we compare different X-ray pump-probe schemes using radiation pulses originating from three different Self-Amplified Spontaneous Emission (SASE) operation modes and additionally from a single-crystal self-seeded mode of the European XFEL. Simulations of the SDL output and the achievable photon energy separation have been performed.

CONCEPTUAL DESIGN

The SDL design is based on symmetric Bragg diffraction from perfect Si (220) crystals. In contrast to grazing incidence mirror optics,[11] this concept is working at large reflection angles, which allows for a more compact design. A schematic layout is presented in Fig. 1.

The incoming FEL pulse is separated in two parts by a beam splitter and the split pulses take two different trajectories along the upper and lower branches of the device. By changing the path length of the upper branch, the difference in arrival times (Δt) between the two pulses can be varied from 0 to the desired 800 ps within a few fs precision. In order to achieve a negative delay time between the two pulses, and thus to allow scanning Δt through the $\Delta t = 0$ position to experimentally determine the temporary overlap, two channel-cut crystals are employed in the lower branch to extend the beam path slightly. This enables negative Δt down to −10 ps, i.e., the lower branch pulse arrives later than the upper branch pulse. A similar design has been proposed and demonstrated by Osaka *et al.*[12] All lower branch elements can be shifted downwards to move away from the X-ray beam

path if desired for non-SDL experiments. In this case, the beam will simply transmit uninterrupted through the vacuum vessel.

Two different concepts can be employed to split the beam. Intensity splitting is achieved by a thin perfect crystal of a few μm thickness[38,39] intersecting the beam. It diffracts a portion of the beam intensity and transmits the remainder. The other concept denoted is geometrical splitting[40] where a thick crystal intersects half of the beam and diffracts that portion, while the other half passes undisturbed over the crystal. This concept has also been recently demonstrated in experiment.[41] The beam merger will be realized using the same concepts to provide two collinear beams. In addition, the beam merger can be adjusted such that a non-collinear beam mode is provided. In this case, the two beams are overlapped at the sample by use of an additional mirror downstream of the SDL which reflects the lower beam upwards, so it hits the same point on the sample as the upper beam. In such an inclined beam mode, the two diffraction patterns resulting from the first and second pulse will be spatially separated on a suitable downstream detector.[7] The two different versions of splitters and mergers are located at different positions along the beam direction, as close to each other as possible. The thin crystal splitter (merger) precedes the geometric splitter (merger). In this way, one can split the beam with the thin crystal and continue in the inclined mode by using a thick crystal merger without reducing the maximum delay time. Equal intensity splitting by a thin crystal requires a splitter of a few μm thickness. Given the current technological difficulties associated with the fabrication and stable operation of thin perfect crystals, geometrical splitting by thick crystals will be the initial operation mode with intensity splitting as a possible future upgrade.

The incident beam size at the SDL varies between 2.7 mm and 0.11 mm at 5 keV and between 1.6 mm and 0.07 mm at 10 keV (calculated) depending on the specific focusing scheme.[16] The two output beams have the same size in the optical splitting case, while the ratio of the two output beam sizes (and thereby the intensity ratio) can be tuned in the geometrical splitting case.
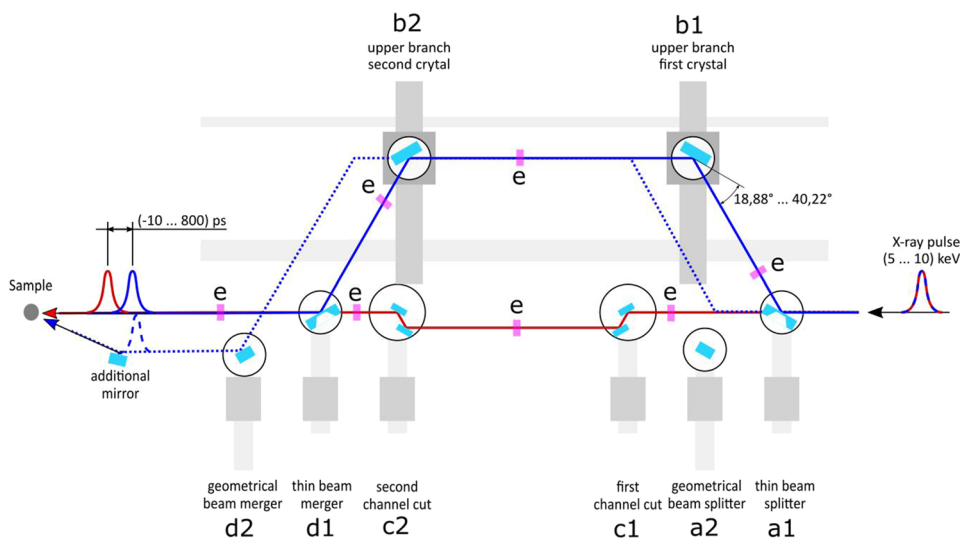

FIG. 1. Schematic layout of the split and delay line. (a1 and a2) beam splitters; (b1 and b2) upper branch crystals; (c1 and c2) channel cuts; (d1 and d2) beam merger; and (e) motorized beam intensity detectors. The upper branch crystals define a trapezoid where the slope of the sides is given by the Bragg angle (and hence the photon energy) and the height is determined by the delay Δt. The blue solid line represents the intensity splitting scheme and the dotted line represents the alternative beam path if the geometrical splitting is applied in a non-collinear beam mode.
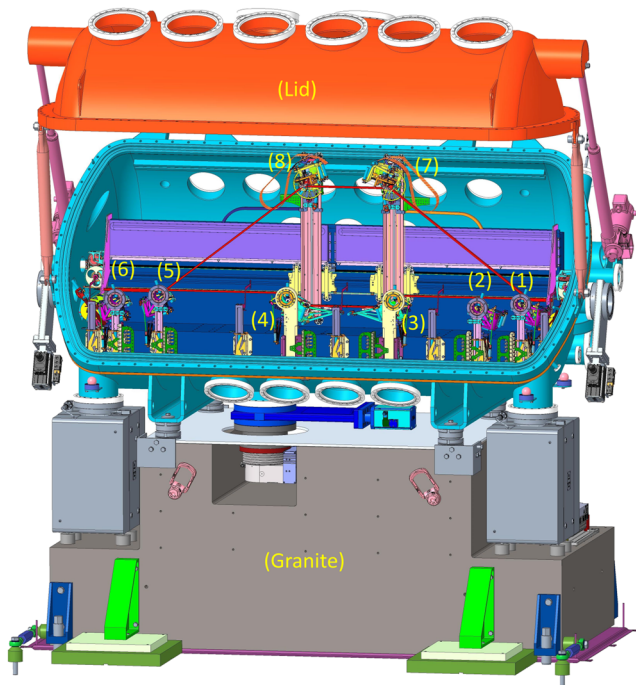
FIG. 2. Mechanical design of the SDL. (1) geometrical beam splitter unit, (2) intensity beam splitter, (3) first channel-cut unit, (4) second channel-cut unit, (5) intensity beam merger unit, (6) geometrical beam merger unit, (7) first delay crystal unit, and (8) second delay crystal unit. X-ray beam paths are indicated by the red line.

TECHNICAL DESIGN

The SDL will be permanently installed at the MID station and is available for user experiments as a default operating option of the instrument. The device is located at the end of the MID optics hutch, about 8 m upstream of the sample position. This location is downstream of a pre-monochromator that reduces the heat load on the first beam splitter crystal. Furthermore, given the space constraints, this position is as close as possible to the sample, which is advantageous for maximum beam stability.

To allow windowless operation of the beamline and reduced contamination of the optical elements, the SDL will be situated in a particle free ultra-high vacuum environment. In Fig. 2, we present an overview of the mechanical design of the SDL with the vacuum vessel containing a custom made optical bench. The vacuum vessel is about 2 m in length and supported by a massive granite block to ensure mechanical stability of the setup. For installation and maintenance purposes, the cylindrical chamber has a hinged lid which is opened by

two lift drives (each left and right). In the fully open state, it can be secured by two safety pillars preventing sudden closure. This provides easy access to the in-vacuum mechanics of the device. In the closed state, the chamber features a very high mechanical stability combined with a minimum of mass, due to its cylindrical shape. The L-shaped optical bench inside the vessel acts as a supporting structure for the precision mechanics and other components. It is designed for high stiffness, and special care was taken in the design to ensure direct mechanical connection between the optical bench and the granite block with minimum coupling to the vessel. As a consequence, this design prevents mechanical and thermal disturbances from the environment to reach the precision mechanics placed on the bench.

The most challenging aspect of the SDL design is the in-vacuum mechanics required to position the optical elements. It must fulfil two demands that are difficult to satisfy simultaneously. First of all, the system must provide large range motions in distance and angle for adjustment to the desired photon energy, the time delay, and the different splitting/merging options. At the same time, a precise alignment is required with a resolution in the range of a few hundred nanometer and a few tens of nanoradian. This is needed in order to set a precise time delay with a few femtoseconds precision and to achieve spatial overlap of the two split beams (down to 10 μm in size) at the sample position 8 m downstream. Table I summarizes the specifications for these motions and their accuracies.

These requirements are achieved by a combination of coarse long range motion axes with fine alignment platforms (FAPs). The FAPs are on top of the long range coarse motion axes. They have been designed to allow for compensation of the parasitic error motions and to move the Si crystals with the required precision. The FAPs are based on the Cartesian parallel kinematic concept with six degrees of freedom.[42]

The coarse long range angular motion is guided by four point ball bearings with stainless steel races, ceramic balls, and Polyether ether ketone (PEEK) cages. It is driven by a stepper motor with a gear head and a lead screw which is tangentially arranged to the axis of rotation. The beam splitter (1, 2 in Fig. 2), merger (5, 6), and the channel cut platforms (3, 4) in the lower optical branch are mounted on the lower vertical side of the optical bench. They are mounted on vertical translation stages with the purpose of clearing all optics from the beam path when beam-splitting is not required and the SDL is switched to a transparent mode. These vertical stages are elastically preloaded gliding carriage systems driven by a lead screw and a stepper motor with gear head from Faulhaber GmbH.

TABLE I. Specifications of the in-vacuum motions.

Crystal	Degrees of freedom (full stroke/accuracy)				
	Bragg angle (pitch)	Roll	X (horizontal)	Y (vertical)	Z (beam direction)
Splitters	18.8°- 40.2°/0.1 μrad	±1°/0.2 μrad	±5 mm/1 μm or better	±10 mm/1 μm or better	None
Channel-cuts	18.8°- 40.2°/0.1 μrad	±1°/0.2 μrad	±5 mm/1 μm or better	±12.5 mm/1 μm or better	None
Mergers	18.8°- 40.2°/0.1 μrad	±1°/0.2 μrad	±5 mm/1 μm or better	+10 ∼ −35 mm/1 μm or better	None
Upper branch crystals	18.8°- 40.2°/0.1 μrad	±1°/0.2 μrad	±5 mm/1 μm or better	0-500 mm/1 μm or better	0-500 mm/1 μm or better

The long range translational motion on the delay branch of the beam path is implemented by a linear guide system in horizontal and vertical direction with gliding carriages. Small pads made of PEEK are embedded into the carriages for gliding on a specially shaped guide way made of aluminum. This material combination minimizes the friction and abrasion and is lightweight and stiff yielding a high eigenfrequency of the structure. The pads are arranged for a statically simple determination of the carriage position, avoiding random tilting and ensuring the highest possible position reproducibility. The guiding contact surfaces of the horizontal and vertical profile rails are arranged to be free of play without additional static preloading by springs. Only gravity ensures the permanent contact of each gliding pad of the carriages to the guide ways. The location where the driving force is applied to the carriages is chosen for a minimum impact to the balance of forces. The minimized friction leads to a small heat emission at the contact points and at the *in situ* stepper motor, allowing for a minimum of both thermal disturbance and stick-slip behavior. We developed these guide systems to provide smooth movements with high resolution, particle free UHV-compatibility as well as stability, and durability for the linear position system of the crystals.

For the long translations of the two upper branch crystal FAPs (7, 8 in Fig. 2) which provide the desired time delay, a special driving system has been developed as shown in Fig. 3. The two rails for guiding the horizontal directions are mounted on the vertical part of the L-shaped bench as can be seen in Fig. 2. The horizontal carriage attaches to these rails and supports the vertical rail to guide the carriage for FAP. To cover the desired time delay of up to 800 ps at 10 keV, strokes of 450 mm in the vertical and 850 mm in the horizontal direction are required. The horizontal translation is driven by a stepper motor through a lead screw. The vertical translation is realized by a rope system. The driving disc of the rope system is mounted on the shaft of the gear head and driven by a stepper motor. The vertical carriage is hanging on the upper part of the rope with its upper pulley and is smoothly preloaded by the lower part of the rope on its lower pulley. It will move vertically upwards just when the driving disc shortens the upper part of the rope and extends the lower part by rotating and

vice versa. The important feature of this arrangement is that the vertical carriage does not move up and down, while the horizontal carriage is moving left and right. The rope runs over the upper and lower pulleys without changing its vertical length component, and hence, the carriage maintains its vertical position while it translates horizontally. The horizontal motion has a full step resolution of 1.9 μm and the vertical translation of 2.2 μm. This implementation hence realizes the upper FAP motion along the steep sides of the trapezoid as two separate horizontal and vertical motions. The important aim is that all motors can be installed at fixed positions inside the vacuum chamber. This allows for a better mechanical stability and implementation of motor cooling without the need for braids and cooling pipes which otherwise would have to move together with the carriages. Linear encoders with nm resolution will be installed for all translations of the upper branch.

Considering the 8 m distance between the SDL and the sample, and in turn the detector being approximately another 8 m (variable) downstream of the sample, we demand a lateral beam stability amounting to 10%-20% of the beam FWHM (approx. 10 μm at the sample) in a typical focusing scheme.[16] This translates to alignment accuracies of 0.1 μrad in the pitch angle (vertical beam shift) and 0.2 μrad in the roll angle (horizontal beam shift) for all the Bragg crystals. Such positioning tolerances can be achieved in the lower branch by utilizing very accurate goniometers and translation units.[43,44] However, for the upper branch FAPs which are the most frequently moving parts of the system, a light weight design is required, posing a challenge with respect to stability. For this purpose, a light weight FAP has been developed that is applicable to all crystals of the SDL.

One FAP contains either 10 or 12 small stepper motors for sufficiently precise control using parallel kinematics. Therefore, the whole SDL system features more than 100 in-vacuum stepper motors. An example of the FAP design is shown in Fig. 4, together with the prototype assembly that has been used to assess the mechanical performance. The coarse pitch alignment of the outer cage (purple) can be adjusted in a range from 18.8° to 40.2° corresponding to the Si (220) Bragg angle from 10 to 5 keV. The angle can be further decreased to
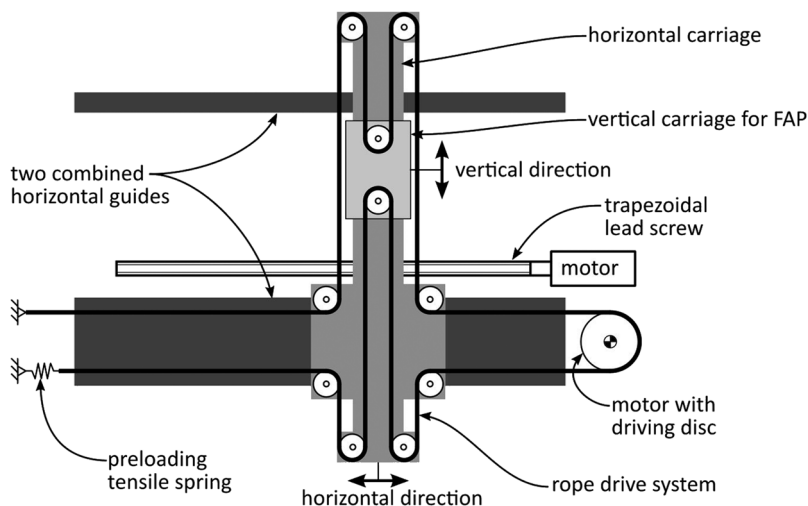

FIG. 3. Concept for driving the coarse translations of the upper branch positioning stages.
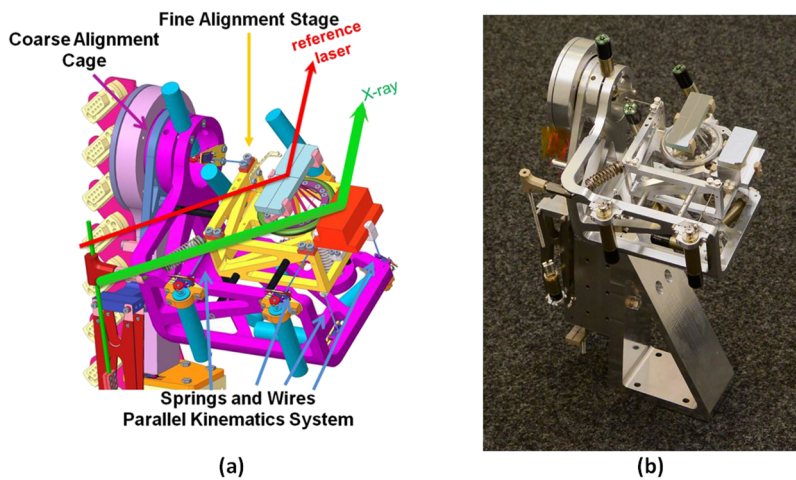
FIG. 4. (a) Model of the fine alignment platform (FAP) hosting the Bragg crystal and a mirror for the reference laser. (b) Photo of the prototype FAP.

(a)   **(b)**

allow operation at higher photon energy, but in this case with smaller maximum time delay. On the outer cage-shaped base, a fine alignment stage [yellow in Fig. 4(a)] is positioned by six stepper motor driven wire winches pulling against a restoring spring force from the left and the bottom side, thus realizing a Cartesian parallel kinematics system.[42] The wires and springs are oriented parallel to the Cartesian coordinates, so complex coordinate transformations are unnecessary hence simplifying the control scheme and improving the precision. The stainless steel ropes of 0.5 mm diameter are coiled on a gear shaft with a ratio of 154 368, providing a resolution of about 2.5 nm per full step. This is the linear resolution for the fine alignment stage. The angular resolution depends on the lever arm defined by the distances between the attachment points of the cables to the stage. For the current design, it amounts to about 36 nrad per full step. The concept of the FAP has been verified using the prototype [Fig. 4(b)] where the inner stage has 6 degrees of freedom and hence complies with the requirements for crystal manipulation inside the SDL. Actual positioning resolution measurements will be performed once the system is mounted in the designed vacuum vessel and the granite support in a low-noise environment.

Due to long travel ranges for the upper branch crystals, parasitic tilt motions cannot be avoided—in fact, we expect them to be up to three orders of magnitude larger than the required alignment accuracies. In order to measure these undesired motions during translations, an *in situ* 3-axis laser interferometer system operating inside the UHV environment has been developed for these two upper branch FAPs. The parasitic tilt displacements of the crystals will be measured by the laser interference signal and corrected for by the FAPs. The resolution of the interferometer is 0.01 μrad (pitch) and 0.02 μrad (roll) which is one order of magnitude better than the crystal alignment requirements. Eventually, we want to combine the interferometry and alignment control system to achieve an automatic ultra-high accuracy position-feedback enabling fast time delay scans with the SDL.

In addition, the SDL features various systems for stabilization, position verification, and alignment. This includes (1) a visible light reference laser that is guided parallel to the FEL beam by reflecting mirrors installed in each crystal cage (see Fig. 4); (2) a temperature stabilization system of the optical

bench including temperature sensors, a cooling scheme, and several heaters at different locations. Space for temperature sensors and cooling of the crystals in the cages is also reserved. The SDL device is placed inside a high precision climate zone with accuracy of 0.1 °C situated inside the optics hutch; (3) thin diamond[45] and Si detectors under development for pulse intensity diagnostics. These motorized beam intensity detectors will be positioned next to each crystal for maintaining the alignment of the crystals and monitoring pulse intensities during the experiment. Moreover, two additional beam position monitors are placed at the entrance and exit of SDL; (4) a control system under development for the coupled motion of several motors simultaneously to change photon energy and/or delay.

OUTPUT SIMULATIONS

In the following, we discuss specifically four different *two-color* hard x-ray pump-probe schemes based on different XFEL configurations and compare their outputs by simulations. The simulations are based on the sketch in Fig. 1 with Si (220) reflections from all crystals and the geometrical wavefront splitting scheme. The crystals in the SDL act as monochromators and reflect photons in a narrow bandwidth $\Delta E/E \sim 6 \times 10^{-5}$ around the desired photon energy E. In the simulations, it is assumed that the SDL introduces a precise (jitter free) relative delay between the two split pulses.

FEL simulations are performed using Genesis 1.3[46] assuming 14 GeV and 250 pC nominal electron beam pulses from start-to-end simulations for the European XFEL[47] yielding a 20 fs FEL pulse at an X-ray photon energy of 8 keV. The photon transmission of the Bragg crystals in the SDL branches is calculated using dynamical diffraction theory in the two-beam approximation, which is implemented in the X-ray optics module of the OCELOT software suite.[48] OCELOT also serves as pre- and post-processor for the FEL simulations. 40 individual FEL pulses were simulated with Genesis for each of the following four FEL radiation configurations: (a) Nominal SASE radiation. (b) Radiation from a Hard X-Ray Self-Seeding (HXRSS)[49] setup where two crystal reflections within the original SASE bandwidth are simultaneously used.[26] (c) SASE radiation from an energy-chirped

electron beam obtained by a corrugated metal structure in the accelerator.[36] (d) SASE radiation using the fresh-slice method.[37] More details about these simulations are presented in another paper in preparation.[50] Here, we concentrate on the output of the SDL device concerning the spectral properties and intensity.

The results of the input and output spectra of the SDL for the four individual cases are presented in Fig. 5. In Figs. 5(a), 5(b), and 5(d), the 40 realizations of the FEL input to the SDL are plotted in gray, while the average is plotted in black. In Fig. 5(c), one simulation of a SASE spectrum takes approximately one day using available computational capabilities. In order to save calculation time, only two full spectra have been simulated and are presented in gray, while 40 runs were performed around the selected smaller energy range of interest, and the average of them is presented in black. The output spectra of the SDL branches are plotted in red and cyan and always have a bandwidth of ~0.6 eV, which is determined by the Darwin width of the Si (220) crystal. In the nominal SASE case presented in Fig. 5(a), the total spectral bandwidth of the FEL pulse is about 50 eV, and the crystals are adjusted to pick up two spectral components with a separation of 8 eV, i.e., separated by 0.1% of the central photon energy. The average output of the SDL for both branches is about 10^{10} photons/pulse. The same output number of photons/pulse in the single-color scheme is expected where the upper and lower branch crystals are tuned to the same Bragg conditions. By inspecting the SASE spectrum, it is obvious that the energy separation can be reduced to obtain higher intensities. Alternatively, the relative weight of the two colors can be tuned by offsetting the SASE spectrum, or the energy separation between the two branches can be increased further at the expense of intensity.

The situation is different in the self-seeded case shown in Fig. 5(b). One uses simultaneously two different crystal reflections in the HXRSS unit in order to obtain two seeded pulses within the original SASE bandwidth. The energy separation is therefore determined by the seeding crystals that define the input spectrum. The crystals in the SDL must be adjusted to the proper angles to reflect the corresponding X-ray pulses and guide them along the two branches of the device. As in the previous case, the energy separation is also limited by the initial SASE bandwidth, but the advantage is a 6 times higher output, about 10^{11} photons/pulse, owing to the increased spectral density of the HXRSS technique.

In case Fig. 5(c), we propose to make use of a corrugated metallic structure in the accelerator[36] introducing a strong energy chirp along the electron beam before it enters the undulator, so that the SASE radiation bandwidth can be effectively broadened. As an example, shown in Fig. 5(c), the SASE bandwidth is increased to about 250 eV and the SDL selects two components with a separation of 140 eV within this bandwidth, which is about 2% of the central photon energy. However, in this case only a limited portion of electrons contributes to the radiation in the selected bandwidth, and the output of the SDL reaches only about 5×10^9 photons/pulse. Finally, in the last case Fig. 5(d), the XFEL radiation pulses are produced using the fresh-slice technique.[37] This method, successfully tested at the Linac Coherent Light Source (LCLS), relies on the fact that while traveling through a corrugated structure, the electron beam is not only chirped, but it also experiences a transverse wake that is a function of the position along the beam. After the corrugated structure, an orbit corrector positions, e.g., the tail of the bunch on a straight lasing path in a first undulator section, while the head experiences betatron oscillations that
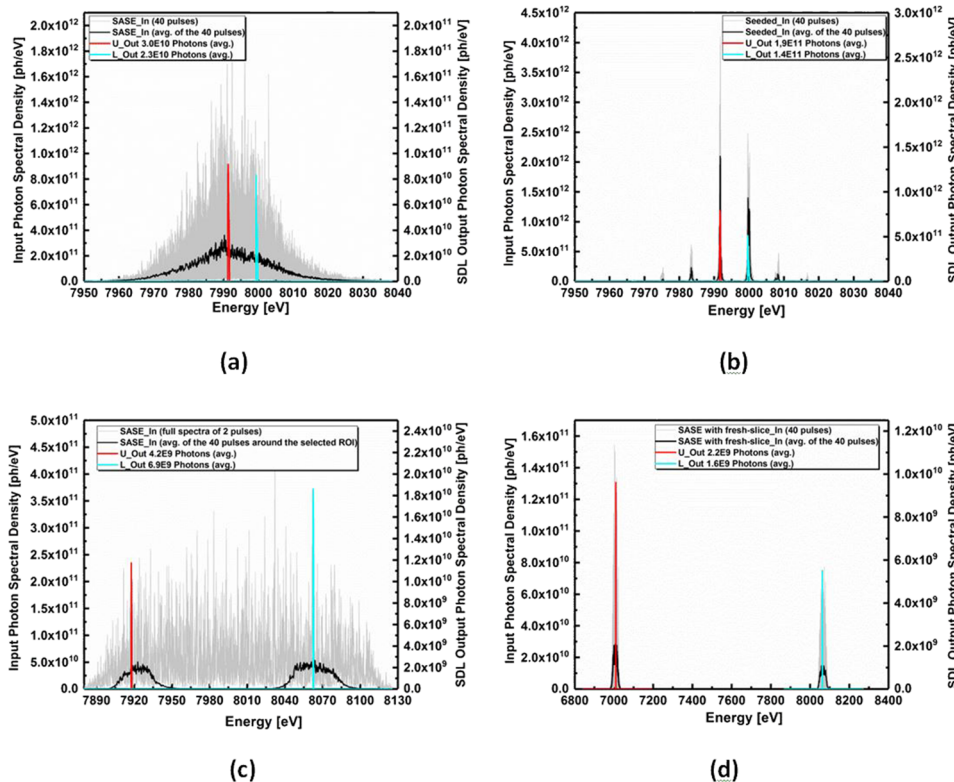

FIG. 5. Simulations for the spectral properties and output of the SDL device (U: upper, L: lower branch). The input spectra of the SDL are presented in gray (individual) and black (average), the outputs of the two branches are presented in red and cyan. The simulations have been performed with (a) nominal SASE radiation, (b) HXRSS radiation using simultaneously two crystal reflections within the original SASE bandwidth, (c) SASE radiation from an energy-chirped electron beam, (d) SASE radiation using the fresh-slice method[37] with an energy-chirped electron beam.

suppress the lasing. A second corrector can now be used to invert the situation in a second undulator so that the head of the bunch radiates, while the tail experiences betatron oscillations. Owing to the adjustable gap of the undulators at the European XFEL, one can set the resonant wavelength of the two undulator parts completely independently. In other words, since the lasing frequency of the tail and of the head of the electron bunch can be independently chosen by different K parameters setting of the two undulator parts, this last method grants the most flexible photon energy separation. The example presented in Fig. 5(d) has a separation of 1.05 keV, thus achieving more than 10% difference between the two pulses. In this case, the photon energies are predefined by the undulator setting and the SDL adapts to them by tuning the crystals, as done in the other cases. The output from the SDL is only about 10^9 photons/pulse, due to the same limitations discussed for case Fig. 5(c) but a much larger energy separation of the two beams can be achieved.

Finally, it must be noted that large pulse-to-pulse fluctuations, about 50%–90% in standard deviation, of the intensity ratio between the two branches are observed in all four cases. This is caused by the spectral randomness that the SASE process generates and also known from our previous work.[18] For experiments that require constant intensity ratios between pulses, this issue can be solved by using intensity monitors in the branches and filtering the data before analysis, selecting only equal or almost equal intensity pairs.

SUMMARY

We present a hard X-ray split-and-delay line for the MID instrument at the European XFEL facility. The device is designed to operate in an energy range from 5 to 10 keV and provides pairs of X-ray pulses with variable delay between −10 and 800 ps in a UHV environment. Options for higher photon energy operation can be implemented. The mechanical concept is guided by the challenging demand of combining large range motion of the optical elements with high precision alignment and resolutions in the nanometer and nanoradian range. A laser interferometer tracking system provides active controls for fine alignment of the optical elements and enables efficient operation while changing the temporal delay.

Based on the SDL device's optical layout in combination with different lasing modes for the European XFEL, four scenarios of two-color operation of the SDL have been proposed and analyzed with respect to the photon energy separation and intensity that can be achieved. In these schemes, both the energy separation and relative arrival times can be varied independently. Our simulations indicate that in all cases, more than 10^9 photons per pulse in both branches will be available downstream of the SDL for two-color experiments. The photon energy separation of the two beams can amount to as much as about 10%. Large pulse-to-pulse fluctuations of the intensity ratio between the two branches are noticed, but post processing according to intensity monitors in the two branches will be possible to select the desired ratio. These features make our setup suitable for novel time-resolved two-color X-ray experiments of the pump-probe or probe-probe type using hard X-ray FEL radiation.

[1] A. Madsen, R. L. Leheny, H. Guo, M. Sprung, and O. Czakkel, New J. Phys. **12**, 055001 (2010).

[2] G. Grübel, G. B. Stephenson, C. Gutt, H. Sinn, and Th. Tschentscher, Nucl. Instrum. Methods Phys. Res., Sect. B **262**, 357 (2007).

[3] W. Roseker, S. O. Hruszkewycz, F. Lehmkühler, M. Walther, H. Schulte-Schrepping, S. Lee, T. Osaka, L. Strüder, R. Hartmann, M. Sikorski, S. Song, A. Robert, P. H. Fuoss, M. Sutton, G. B. Stephenson, and G. Grübel, Nat. Commun. **9**, 1704 (2018).

[4] F. Perakis, G. Camisasca, T. J. Lane, A. Späh, K. T. Wikfeldt, J. A. Sellberg, F. Lehmkühler, H. Pathak, K. H. Kim, K. Amann-Winkel, S. Schreck, S. Song, T. Sato, M. Sikorski, A. Eilert, T. McQueen, H. Ogasawara, D. Nordlund, W. Roseker, J. Koralek, S. Nelson, P. Hart, R. Alonso-Mori, Y. Feng, D. Zhu, A. Robert, G. Grübel, L. G. M. Pettersson, and A. Nilsson, Nat. Commun. **9**, 1917 (2018).

[5] K. E. Schmidt, J. C. H. Spence, U. Weierstall, R. Kirian, X. Wang, D. Starodub, H. N. Chapman, M. R. Howells, and R. B. Doak, Phys. Rev. Lett. **101**, 115507 (2008).

[6] C. M. Günther, B. Pfau, R. Mitzner, B. Siemer, S. Roling, H. Zacharias, O. Kutz, I. Rudolph, D. Schondelmaier, R. Treusch, and S. Eisebitt, Nat. Photonics **5**, 99 (2011).

[7] J. J. van Thor and A. Madsen, Struct. Dyn. **2**(1), 014102 (2015).

[8] S. Roling and H. Zacharias, "Split-and-delay units for soft and hard x-rays," in *Synchrotron Light Sources and Free-Electron Lasers*, edited by E. Jaeschke, S. Khan, J. Schneider, and J. Hastings (Springer, Cham, 2014).

[9] M. Wöstmann, R. Mitzner, T. Noll, S. Roling, B. Siemer, F. Siewert, S. Eppenhoff, F. Wahlert, and H. Zacharias, J. Phys. B: At., Mol. Opt. Phys. **46**, 164005 (2013).

[10] T. Osaka, T. Hirano, M. Yabashi, Y. Sano, K. Tono, Y. Inubushi, T. Sato, K. Ogawa, S. Matsuyama, T. Ishikawa, and K. Yamauchi, Proc. SPIE **9210**, 921009 (2014).

[11] S. Roling, K. Appel, S. Braun, A. Buzmakov, O. Chubar, P. Gawlitza, L. Samoylova, B. Siemer, E. Schneidmiller, H. Sinn, F. Siewert, T. Tschentscher, F. Wahlert, M. Wöstmann, M. Yurkov, and H. Zacharias, Proc. SPIE **9210**, 92100B (2014).

[12] T. Osaka, T. Hirano, Y. Sano, Y. Inubushi, S. Matsuyama, K. Tono, T. Ishikawa, K. Yamauchi, and M. Yabashi, Opt. Express **24**, 9187 (2016).

[13] W. Roseker, H. Franz, H. Schulte-Schrepping, A. Ehnes, O. Leupold, F. Zontone, S. Lee, A. Robert, and G. Grübel, J. Synchrotron Radiat. **18**, 481 (2011).

[14] D. Zhu, Y. Sun, D. W. Schafer, H. Shi, J. H. James, K. L. Gumerlock, T. O. Osier, R. Whitney, L. Zhang, J. Nicolas, B. Smith, A. H. Barada, and A. Robert, Proc. SPIE **10237**, 102370R (2017).

[15] M. Altarelli, R. Brinkmann, M. Chergui, W. Decking, B. Dobson, S. Düsterer, G. Grübel, W. Graeff, H. Graafsma, J. Hajdu, J. Marangos, J. Pflüger, H. Redlin, D. Riley, I. Robinson, J. Rossbach, A. Schwarz, K. Tiedtke, T. Tschentscher, I. Vartaniants, H. Wabnitz, H. Weise, R. Wichmann, K. Witte, A. Wolf, M. Wulff, and M. Yurkov, XFEL Technical Design Report, http://xfel.desy.de/technical_information/tdr/tdr/.

[16] A. Madsen, J. Hallmann, T. Roth, and G. Ansaldi, Technical Design Report of the MID instrument, http://pubdb.xfel.eu/record/154260.

[17] O. Grimm, K. Klose, and S. Schreiber, in *Proceedings of EPAC 2006* (CERN, 2006), p. 3143, available at https://accelconf.web.cern.ch/accelconf/e06/PAPERS/THPCH150.PDF; A. Marinelli, D. Ratner, A. A. Lutman, J. Turner, J. Welch, F.-J. Decker, H. Loos, C. Behrens, S. Gilevich, A. A. Miahnahri, S. Vetter, T. J. Maxwell, Y. Ding, R. Coffee, S. Wakatsuki, and Z. Huang, Nat. Commun. **6**, 6369 (2015).

[18] W. Lu, T. Noll, T. Roth, I. Agapov, G. Geloni, M. Holler, J. Hallmann, G. Ansaldi, S. Eisebitt, and A. Madsen, AIP Conf. Proc. **1741**, 030010 (2016).

[19] B. Friedrich, S. Eisebitt, W. Lu, A. Madsen, T. Noll, and T. Roth, in *Proceedings of the MEDSI2016* (JACoW, 2017), p. MOPE22, availalble at https://doi.org/10.18429/JACoW-MEDSI2016-MOPE22.

[20] I. Inoue, Y. Inubushi, T. Sato, K. Tono, T. Katayama, T. Kameshima, K. Ogawa, T. Togashi, S. Owada, Y. Amemiya, T. Tanaka, T. Hara, and M. Yabashi, Proc. Natl. Acad. Sci. U. S. A. **113**, 1492 (2016).

[21] E. Allaria, F. Bencivenga, R. Borghes, F. Capotondi, D. Castronovo, P. Charalambous, P. Cinquegrana, M. B. Danailov, G. De Ninno, A. Demidovich, S. Di Mitri, B. Diviacco, D. Fausti, W. M. Fawley, E. Ferrari, L. Froehlich, D. Gauthier, A. Gessini, L. Giannessi, R. Ivanov, M. Kiskinova, G. Kurdi, B. Mahieu, N. Mahne, I. Nikolov, C. Masciovecchio, E. Pedersoli, G. Penco, L. Raimondi, C. Serpico, P. Sigalotti, S. Spampinati, C. Spezzani, C. Svetina, M. Trovò, and M. Zangrando, Nat. Commun. **4**, 2476 (2013).

[22] A. A. Lutman, R. Coffee, Y. Ding, Z. Huang, J. Krzywinski, T. Maxwell, M. Messerschmidt, and H.-D. Nuhn, Phys. Rev. Lett. **110**, 134801 (2013).

[23] A. Picón, C. S. Lehmann, C. Bostedt, A. Rudenko, A. Marinelli, T. Osipov, D. Rolles, N. Berrah, C. Bomme, M. Bucher, G. Doumy, B. Erk, K. R. Ferguson, T. Gorkhover, P. J. Ho, E. P. Kanter, B. Krässig, J. Krzywinski, A. A. Lutman, A. M. March, D. Moonshiram, D. Ray, L. Young, S. T. Pratt, and S. H. Southworth, Nat. Commun. **7**, 11652 (2016).

[24] T. Hara, Y. Inubushi, T. Katayama, T. Sato, H. Tanaka, T. Tanaka, T. Togashi, K. Togawa, K. Tono, M. Yabashi, and T. Ishikawa, Nat. Commun. **4**, 2919 (2013).

[25] G. Ninno, B. Mahieu, E. Allaria, L. Giannessi, and S. Spampinati, Phys. Rev. Lett. **110**, 064801 (2013).

[26] A. A. Lutman, F.-J. Decker, J. Arthur, M. Chollet, Y. Feng, J. Hastings, Z. Huang, H. Lemke, H.-D. Nuhn, A. Marinelli, J. L. Turner, S. Wakatsuki, J. Welch, and D. Zhu, Phys. Rev. Lett. **113**, 254801 (2014).

[27] A. Petralia, M. P. Anania, M. Artioli, A. Bacci, M. Bellaveglia, M. Carpanese, E. Chiadroni, A. Cianchi, F. Ciocci, G. Dattoli, D. Di Giovenale, E. Di Palma, G. P. Di Pirro, M. Ferrario, L. Giannessi, L. Innocenti, A. Mostacci, V. Petrillo, R. Pompili, J. V. Rau, C. Ronsivalle, A. R. Rossi, E. Sabia, V. Shpakov, C. Vaccarezza, and F. Villa, Phys. Rev. Lett. **115**, 014801 (2015).

[28] A. Picón, J. Mompar, and S. H. Southworth, New J. Phys. **17**, 083038 (2015).

[29] E. Shwartz and S. Shwartz, Opt. Express **23**, 7471 (2015).

[30] E. Prat, S. Bettoni, and S. Reiche, Nucl. Instrum. Methods Phys. Res., Sect. A **865**, 1 (2017).

[31] Q. Shen, Q. Hao, and S. M. Gruner, Phys. Today **59**(3), 46 (2006).

[32] S. Muniyappan, S. O. Kim, and H. Ihee, Bio. Des. **3**, 98 (2015), available at http://www.bdjn.org/Journal_Prv_View.html?j_sub_num=40.

[33] S. Serkez, V. Kocharyan, E. Saldin, I. Zagorodnov, G. Geloni, and O. Yefanov, in *Proceedings of FEL2013* (CERN, 2013), available at http://accelconf.web.cern.ch/AccelConf/FEL2013/papers/wepso63.pdf.

[34] P. Emma, M. Venturini, K. L. F. Bane, G. Stupakov, H.-S. Kang, M. S. Chae, J. Hong, C.-K. Min, H. Yang, T. Ha, W. W. Lee, C. D. Park, S. J. Park, and I. S. Ko, Phys. Rev. Lett. **112**, 034801 (2014).

[35] E. Prat, M. Calvi, and S. Reiche, J. Synchrotron Radiat. **23**, 874 (2016).

[36] I. Zagorodnov, G. Feng, and T. Limberg, Nucl. Instrum. Meth. A **837**, 69 (2016).

[37] A. A. Lutman, T. J. Maxwell, J. P. MacArthur, M. W. Guetg, N. Berrah, R. N. Coffee, Y. Ding, Z. Huang, A. Marinelli, S. Moeller, and J. C. U. Zemella, Nat. Photonics **10**, 745 (2016).

[38] W. J. Bartels, J. Hornstra, and D. J. W. Lobeek, Acta Crystallogr., Sect. A: Found. Crystallogr. **42**, 539 (1986).

[39] T. Osaka, M. Yabashi, Y. Sano, K. Tono, Y. Inubushi, T. Sato, S. Matsuyama, T. Ishikawa, and K. Yamauchi, Opt. Express **21**, 2823 (2013).

[40] S. Roling, L. Samoylova, B. Siemer, H. Sinn, F. Siewert, F. Wahlert, M. Wöstmann, and H. Zacharias, Proc. SPIE **8504**, 850407 (2012).

[41] T. Osaka, T. Hirano, Y. Morioka, Y. Sano, Y. Inubushi, T. Togashi, I. Inoue, K. Tono, A. Robert, K. Yamauchi, J. B. Hastings, and M. Yabashi, IUCrJ **4**, 728 (2017).

[42] T. Noll, K. Holldack, G. Reichardt, O. Schwarzkopf, and T. Zeschke, Precis. Eng. **33**, 291 (2009).

[43] D. Shu, T. S. Toellner, and E. E. Alp, Nucl. Instrum. Methods Phys. Res., Sect. A **467**, 771 (2001).

[44] A. Chumakov, R. Rüffer, O. Leupold, J.-P. Celse, K. Martel, M. Rossat, and W.-K. Lee, J. Synchrotron Radiat. **11**, 132 (2004).

[45] T. Roth, W. Freund, U. Boesenberg, G. Carini, S. Song, G. Lefeuvre, A. Goikhman, M. Fischer, M. Schreck, J. Grünert, and A. Madsen, J. Synchrotron Radiat. **25**(1), 177 (2018).

[46] S. Reiche, Nucl. Instrum. Methods Phys. Res., Sect. A **429**, 243 (1999).

[47] I. Zagorodnov, S2e simulations, DESY MPY Start-to-End Simulations page, http://www.desy.de/fel-beam/s2e/xfel.html.

[48] I. Agapov, G. Geloni, S. Tomin, and I. Zagorodnov, Nucl. Instrum. Methods Phys. Res., Sect. A **768**, 151 (2014).

[49] G. Geloni, V. Kocharyan, and E. Saldin, J. Mod. Opt. **58**, 1391 (2011).

[50] K. Zhou, G. Geloni, S. Serkez, W. Lu, A. Madsen, and D. Wang, "Enabling flexible two-color operation with the split-and-delay line at the European XFEL" (unpublished).